ACS APPLIED MATERIALS & INTERFACES

LETTER

www.acsami.org

Shape-Independent Lateral Force Calibration

Evan V. Anderson, Saonti Chakraborty, Taylor Esformes, Derek Eggiman, Colin DeGraf, Keeley M. Stevens, Deli Liu, and Nancy A. Burnham*

Physics Department, Worcester Polytechnic Institute, 100 Institute Road, Worcester, Massachussetts 01609, United States

Supporting Information

ABSTRACT: Current methods for lateral force calibration are often time-consuming, expensive, or cause significant wear of the tip. A quick and simple alternative is presented in which the linear relationship between force and voltage is exploited. The technique is independent of the shapes of the sample and cantilever and eliminates common problems, while maintaining better than 10% precision. This advance will facilitate quantitative comparisons between experiments.

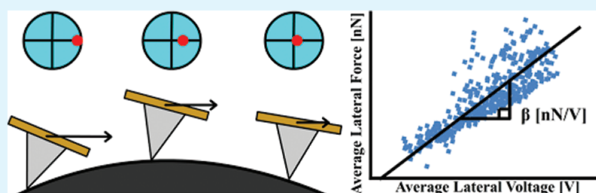

KEYWORDS: force microscopy, calibration, nanocharacterization, tribology, friction

Also known as friction force microscopy, lateral force microscopy (LFM) is a technique used to make friction measurements on the micro- and nanoscales. Instead of observing topography with the vertical deflection of the cantilever as in traditional atomic force microscopy (AFM), the lateral deflection or twisting of the cantilever is observed. The lateral force on the cantilever provides information about the friction between the tip and sample.

LFM has been key to experimental[1−3] and theoretical[4,5] developments in tribology and a wide variety of applications in chemistry, physics, and biotechnology on the nanoscale. Cantilevers with low lateral spring constants can provide friction resolution as high as 10 picoNewtons, which is roughly the force required to "unzip" DNA.[6,7] LFM has been used to measure lateral bonding strength by functionalizing the tip with one chemical and the surface with another,[8,9] and to investigate the critical shear force needed to dislodge bacteria such as *Staphylococcus aureus*[10] and *Pseudomonas aeruginosa*.[11] LFM is being applied to systems where friction must be minimized, such as microelectromechanical systems (MEMS)[12] and nanoelectromechanical systems (NEMS),[13] and to more novel applications such as the characterization of damaged and conditioned human hair.[14,15]

The primary problem with LFM has been the difficulty in calibrating the cantilever and tip in order to obtain quantitative data; researchers have often been limited to qualitative relative comparisons. Several review[6,16,17] and research articles[15,18] have expressed this difficulty and the need for a simple, universally accepted method. A quick and simple quantitative approach would enable the comparison of nano- and macroscale friction studies.

The available procedures have numerous limitations. Some require specialized samples or setups.[19−23] Others are difficult to perform.[24−27] A number of them are indirect, or only suitable for certain cantilevers.[21,24−26,28] Several risk damage to the tip or sample, or both, and might require the geometry of the cantilever, which can be time-consuming to measure.[23,27,29,30]

Proposed here is a new calibration technique that alleviates the aforementioned problems. It is independent of the shape of the sample and cantilever, requires only one set of images (minimizing tip wear and calibration time), is independent of scan parameters including load force, scan rate, and gain, and its precision is better than 10%. The entire calibration process can be as fast as fifteen minutes depending on the instrument, and a majority of this time is spent calibrating the normal (perpendicular to the plane of the cantilever) spring constant.

The construction of our model begins by relating the coordinate axes of the cantilever and arbitrarily shaped sample to that of the scanner. If the axes of the scanner are $i-j-k$ (Figure 1A) and the cantilever is in the $j-k$ plane, the cantilever axes are obtained by rotating through an angle φ about the i axis. Similarly, the axes of the sample are obtained by first rotating through an angle θ about the $-j$ axis to obtain k' (an intermediate transformation axis) and p (Figure 1B) and then rotating through an angle α

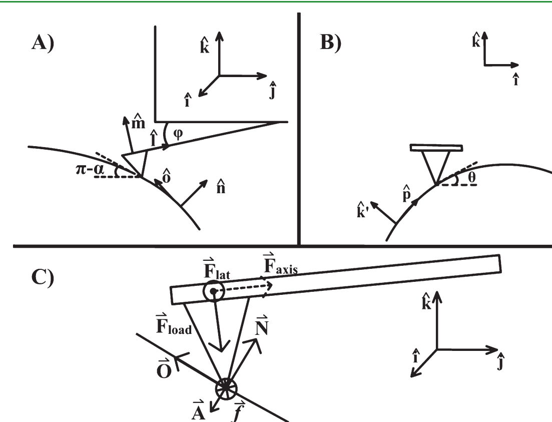

Figure 1. This diagram illustrates the coordinates and forces involved in the model. (A) Fast-scan perspective with scanner (i,j,k), cantilever (l,m), and sample axes (n,o) in the $j-k$ plane. (B) Slow-scan perspective showing the sample axis, p, and intermediate axis, k', in the $i-k$ plane. (C) Free-body diagram depicting the forces on the cantilever tip. The definitions of the forces are given in the text.

Received: June 15, 2011
Accepted: August 19, 2011
Published: August 19, 2011

ACS Publications © 2011 American Chemical Society

dx.doi.org/10.1021/am200770r | ACS Appl. Mater. Interfaces 2011, 3, 3256–3260

about $+p$ to obtain n and o (Figure 1A). These rotations are all counterclockwise. This gives the following set of unit vectors: i, the fast-scan direction of the scanner, j, the slow-scan direction of the scanner, k, the vertical axis of the scanner, l, the direction of the cantilever long-axis, m, the direction normal to the cantilever, n, the direction normal to the sample, p, the direction of the path of the tip in the plane of the sample in the $i-k$ plane, and o, the direction mutually orthogonal to n and p. The relations between these vectors and the scanner axes are shown in eqs 1−5.

$$\hat{l} = \cos\varphi\hat{j} + \sin\varphi\hat{k} \tag{1}$$

$$\hat{m} = -\sin\varphi\hat{j} + \cos\varphi\hat{k} \tag{2}$$

$$\hat{n} = -\cos\alpha\sin\theta\hat{l} - \sin\alpha\hat{j} + \cos\alpha\cos\theta\hat{k} \tag{3}$$

$$\hat{o} = \sin\alpha\sin\theta\hat{l} - \cos\alpha\hat{j} - \sin\alpha\cos\theta\hat{k} \tag{4}$$

$$\hat{p} = \cos\theta\hat{l} + \sin\theta\hat{k} \tag{5}$$

Amontons' Law is assumed for friction; the force of friction is proportional to the sum of the normal force and adhesion, as seen in eq 6.

$$f = \mu(N + A) \tag{6}$$

Although future versions of this model could accommodate alternative friction laws, this assumption often holds at the nanoscale.[31]

The next step is to sum the forces in the i, j, and k directions and impose equilibrium conditions. The free-body diagram of the forces on the tip can be seen in Figure 1C. Only three variables may be solved for because there are only three equilibrium equations. The equilibrium equations for the $i-j-k$ directions are:

$$\sum F_x = F_{lat} + O\sin\alpha\sin\theta - (N - A)\cos\alpha\sin\theta \mp \mu(N + A)\cos\theta = 0 \tag{7}$$

$$\sum F_y = F_{load} + \sin\varphi - O\cos\alpha - (N - A)\sin\alpha + F_{axial}\cos\varphi = 0 \tag{8}$$

$$\sum F_z = -F_{load}\cos\varphi - O\sin\alpha\cos\theta + (N - A)\cos\alpha\cos\theta \mp \mu(N + A)\sin\theta + F_{axial}\sin\varphi = 0 \tag{9}$$

Here F_{lat} is the lateral force, F_{load} is the load force, F_{axial} is the force along the axis of the cantilever, φ is the cantilever angle of repose, O is the force in the o direction, N is the normal force, A is the adhesion force, μ is the coefficient of friction, and α and θ are the sample angles. Using these equations, the lateral force in the forward and reverse directions can be solved for, as shown in eq 10.

$$F_{lat\pm} = \frac{F_{load}}{(1 \mp \mu\cos\alpha\tan\theta)}[\cos\varphi\tan\theta \pm \mu(\cos\alpha\cos\varphi + \sin\alpha\sin\varphi\sec\theta)] \pm \frac{2\mu A\sec\theta}{(1 \mp \mu\cos\alpha\tan\theta)} - \frac{F_{axial}}{(1 \mp \mu\cos\alpha\tan\theta)}[2\tan\alpha\cos\varphi\sin\theta + \sin\varphi\tan\theta \pm \mu\cos\theta(\sin\alpha\cos\varphi + \cos\alpha\sin\varphi\sec\theta)] \tag{10}$$

The axial term is small because it contains the small angles α and φ and because the fast-scan direction is orthogonal to the long axis of the cantilever; the axial term it is therefore subsequently neglected.

For comparison with earlier work, if the angle of repose, φ, and the angle of the sample in the y-direction, α, are also set to zero, eqs 5 and 6 of Varenberg are almost recovered.[21] There is a small difference (a factor of 2) in the adhesion term; this stems from the difference in assumptions of the friction law. In Varenberg's paper, friction force was $f = \mu N$; here it is $f = \mu(N+A)$. The discrepancy is small, as in both cases the term is multiplied by μ. Yet by allowing α and φ to be nonzero and the subsequent necessity of including the orthogonal force O, the more general case is developed here. Furthermore, the axial term has not been previously treated.

Continuing on, the average and difference between the lateral force from forward and reverse scans are shown in eqs 11 and 12, respectively.

$$\bar{F}_{lat} = F_{load}\cos\varphi\tan\theta\left[\frac{1 + \mu^2\cos^2\alpha(1 + \tan\alpha\tan\varphi\sec\theta)}{1 - (\mu\cos\alpha\tan\theta)^2}\right] + 2A\left[\frac{\mu^2\cos\alpha\tan\theta\sec\theta}{1 - (\mu\cos\alpha\tan\theta)^2}\right] \tag{11}$$

$$\Delta F_{lat} = \frac{2\mu}{\cos\theta}\left[\frac{F_{load}\cos\varphi\cos\alpha(\sec\theta + \tan\varphi\tan\alpha) + 2A}{1 - (\mu\cos\alpha\tan\theta)^2}\right] \tag{12}$$

Equation 11 is the primary equation of interest because it is used to find the calibration factor, β, and intercept, γ, using the linear relationship between the average lateral force, $\bar{F}_{lat}$, and the average lateral voltage, $\bar{V}_{lat}$, as shown in eq 13.

$$\bar{F}_{lat} = \beta\bar{V}_{LFM} + \gamma \tag{13}$$

Use of a sample with a large range of angles will yield a more accurate calibration factor because of the wider range of data used to find the slope in the force-voltage plot.

Our calibration program (described in the Supporting Information) implements eqs 11 and 12. It requires the measurement of the normal spring constant, z-scanner displacement, and average adhesion. The normal spring constant was calibrated by using the resonance frequency of the cantilever from a thermal spectrum as described by Matei et al.[32] The average adhesion between the tip and sample was found by acquiring 16 force curves along the apex of a pulled micropipettes, equally spaced along the length of the image.

Pulled micropipettes are recommended as samples for their ease of use, availability, low cost, and wide range of sample angles. They are also easily made from normal micropipettes by heating the center and pulling the ends apart. The pipettes are placed in the AFM with their long axes perpendicular to the fast-scan direction, which is orthogonal to the long axis of the cantilever. If larger sample angles are desired, one moves down the pipet; if the angles are too steep for stable imaging, one moves up the pipet. Although a pipet is convenient, any sample with at least two slopes may be used, unlike earlier work in which the shape of a sample with known slope(s) is prescribed.[21,22,28]

Each experiment was performed in a similar fashion by using a pyramid-type variation of parameters. For example, the set point of the force was varied from 0 to −7 V in increments of 1 V, and

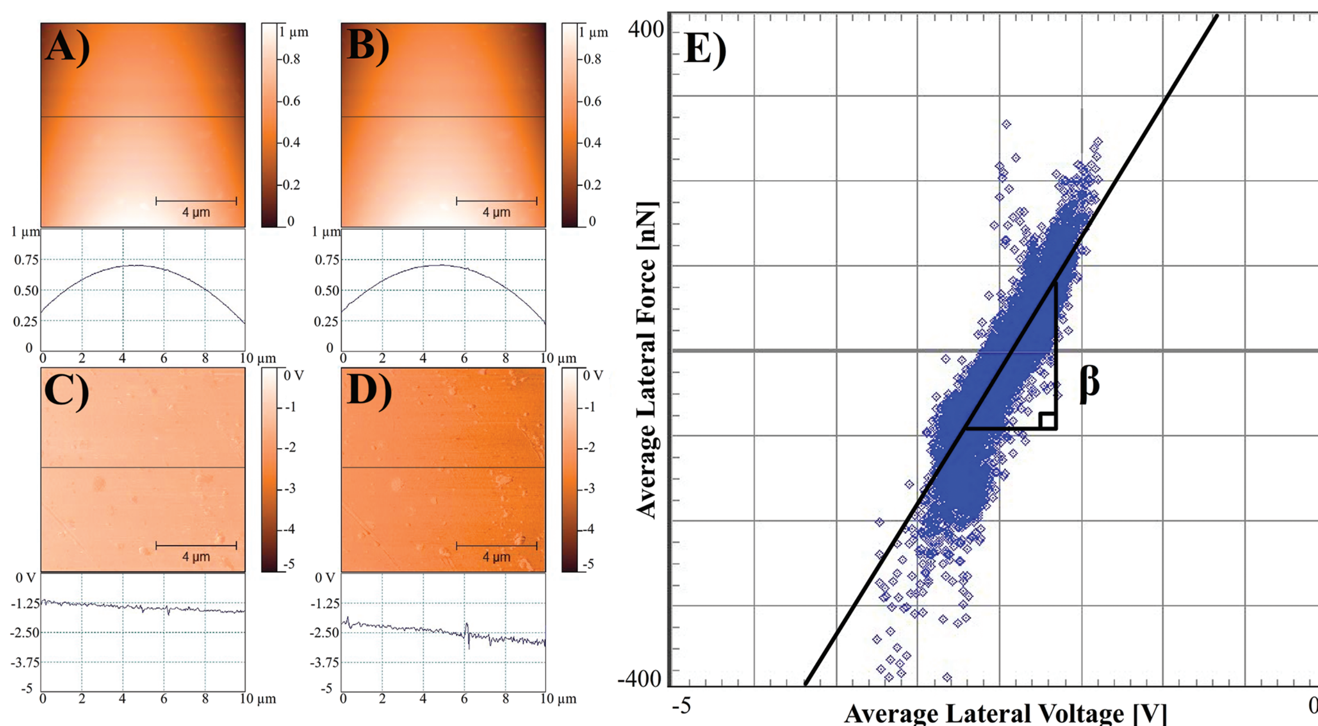

Figure 2. Typical set of images, cross-sections across the middles of the images, and a calibration plot are shown for a pulled micropipette. (A) Forward and (B) reverse topography, for which the angle in the **i**−**k** plane ranges from +9° to −10°. (C) Forward and (D) reverse lateral force in volts, where the cross sections are linear because the response is dominated by the first term in eq 10, which is linear for the range of angles in A and B. (E) Plot of the average lateral force in nanoNewtons against the average lateral voltage in Volts for the 65,536 datum points; the slope of the straight-line fit is the calibration factor β. The calibration factor and intercept can then be used to convert the lateral force voltage into a quantitative force. The calibration factor and intercept for this example are 313 nN/V and 624 nN, respectively.

then back down to 0 in the same manner until three data points had been acquired for each set point. The scan rate and gain were varied the same way until four data points were collected. A set point of −5 V was typical for these experiments. The effect of sample wear was tested by allowing the AFM to scan for 70 min, resulting in 16 sets of images and consequently 16 calibration factors. To investigate the influence of sample shape, two areas on the micropipette were imaged that had drastically different radii of curvature. Five sets of images were taken at each radius. More experimental details are given in the Supporting Information.

Figure 2A−D shows a typical set of images (forward and reverse topography and LFM) of a pulled micropipette. Figure 2E shows an example calibration plot (LFM voltage on the *x*-axis, eq 11 on the *y*-axis) which gives the calibration factor, β, and the intercept, γ, needed to convert the lateral signal from Volts to nanoNewtons (eq 13).

There were several things to test to ensure the validity of this technique including the calibration factor's dependence on: the shape of the sample and cantilever, load force, scan rate, gain, repeatability, precision, and accuracy. The calibration factor should be independent of the scan parameters, be repeatable, and have good precision and accuracy. On average, the calibration factor varied by about 7% between images taken on the same sample. The accuracy of the calibration was tested at an order-of-magnitude level by comparing lateral spring constants found experimentally with those found geometrically (see Calibration Accuracy section of the Supporting Information). They were within 65% of each other.

The calibration factor was assumed to be independent of sample topography because the lateral force is calculated based on the measured slopes of the sample. Theoretical test files were generated that model the topography and lateral voltage signal of a cone and a sphere. When run through the calibration program, these files produced a perfectly linear plot of lateral force against lateral voltage; the calibration factors were the same. This assumption was also tested by imaging a pulled-micropipette at two different radii of curvature—the larger of which had very rough topography—and the calibration factors were statistically equivalent, as seen in Figure 3. Although the two different sets of images are from the same sample, the topography was different enough to conclude that the calibration factor was independent of sample shape.

The relationship between the average lateral force and average lateral voltage must be linear in order that this approach be valid. Linearity depends on the deformation profile of the cantilever, the linearity of the photodetector's response, and the profile of the reflected laser light at the photodetector. To date, all cantilevers tested have behaved linearly; this method is thus far independent of cantilever geometry.

Figure 4A shows normalized calibration factors as a function of the scan parameters (load force, scan rate, and gain). The calibration factor was found to be independent of each of these parameters as seen from the error bars. The only point of concern is the statistically significant lower calibration factor for a set point of 0 V. Error analysis of the lateral force equations suggests that there is a significantly larger error in the calibration factor at zero load-force (see the Error Analysis section of the Supporting

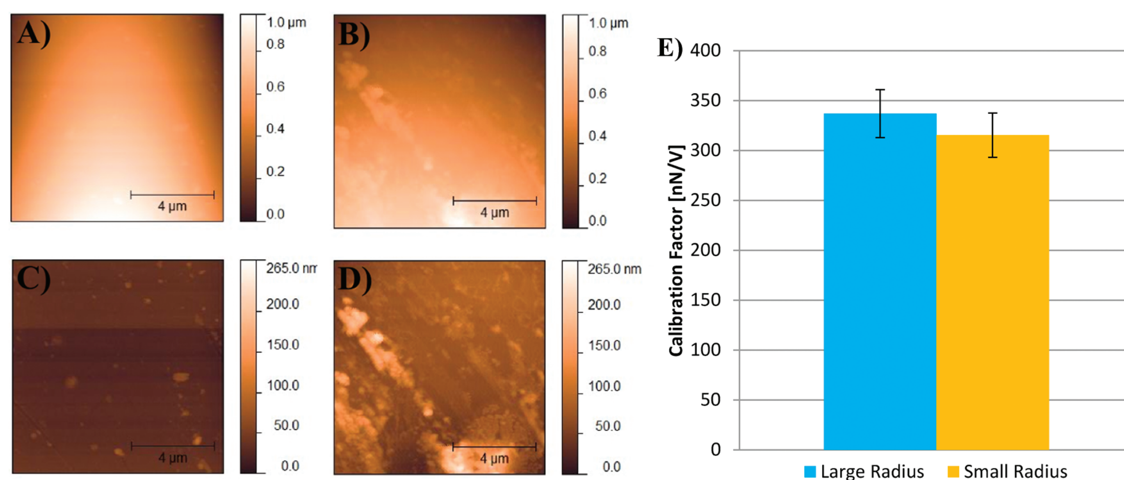

Figure 3. Forward topography at (A) small radius (28.9 μm) and (B) large radius (98.1 μm) of a pulled micropipet. Leveled images of (C) small radius and (D) large radius to show the large difference in local topography. The rms roughness of C is 4.4 nm, and for D it is 24.2 nm. (E) Shape-independence is shown from calibration factors found from A and B, which differ in radius as well as local topography. The calibration factor is independent of sample shape because the lateral force is calculated from the measured slopes of the sample surface. The averages and standard deviations are calculated from five sets of images.

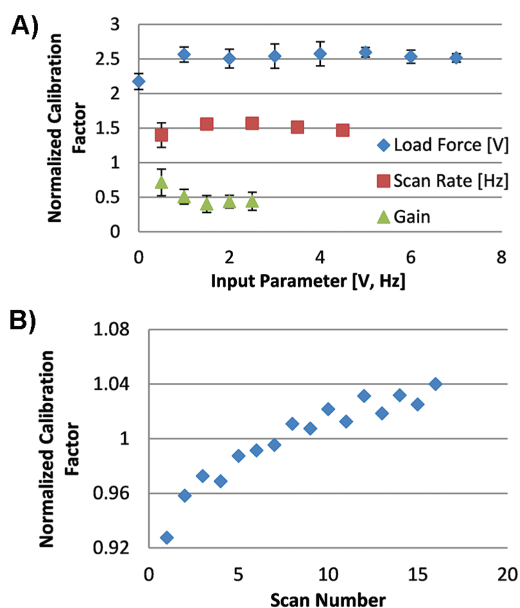

Figure 4. Parameters for which the calibration factor β was (A) independent and (B) dependent. The calibration factors have been normalized to one and are unitless. The normalized calibration factors for each parameter in A were offset for clarity. The calibration factor at zero load force was statistically smaller, possibly because of the error in the measured adhesion (see the Supporting Information). The number of samples used to calculate error are 3, 5, and 5 for the load force, scan rate, and gain respectively. The error bars cannot be seen in some cases because they are obscured by the data points. This shows that the calibration factor was independent of load force, gain, and scan rate. (B) The calibration factor increased slightly with each subsequent set of images, probably because of wear of the tip.

Information). Figure 4B shows the behavior of the calibration factor as a function of scan number. The slight increase in calibration factor for each subsequent image is probably due to wear of the tip.[33] The standard deviation of the calibration factor among the 16 sets of images is only about 3%. Yet only one set of images—or even a set of partial images—is needed in order to obtain the calibration factor. A description of successful calibration with partial images can be found in the Tip Wear section of the Supporting Information.

This calibration technique has been shown to produce precise (<10%) calibration factors independent of shape (Figure 3), load force, gain, and scan rate (Figure 4A) in a quick and simple manner, which will enable better comparisons of nano- and macroscale friction data. By basing the technique on the measured angles of a sample, instead of on a sequence of loads, the calibration requires only one set of images.[28] The entire calibration process can take as little as fifteen minutes and is primarily limited by the time taken to calibrate the normal spring constant of the cantilever. Future work includes determining the accuracy, investigating partial imaging, comparing with other techniques, and determining friction coefficients for standard combinations of tip and sample materials. An investigation of the effects of crosstalk as others have done is also important.[6,16] The ultimate goal is to make the calibration traceable to national measurement laboratories, such as the National Institute of Standards and Technology.

ASSOCIATED CONTENT

Supporting Information. Information regarding the calibration program, the calibration's accuracy, error analysis, tip wear, interpretation of the coefficient of friction, along with further experimental details. This material is available free of charge via the Internet at http://pubs.acs.org/.

AUTHOR INFORMATION

Corresponding Author
*E-mail: nab@wpi.edu.

REFERENCES

(1) Lee, C.; Li, Q.; Kalb, W.; Liu, X.; Berger, H.; Carpick, R.; Hone, J. *Science* **2010**, *328*, 76–80.

(2) Park, J.; Ogletree, D.; Thiel, P.; Salmeron, M. *Science* **2006**, *313*, 186–186.

(3) Liley, M.; Gourdon, D.; Stamou, D.; Meseth, U.; Fischer, T.; Lautz, C.; Stahlberg, H.; Vogel, H.; Burnham, N.; Duschl, C. *Science* **1998**, *280*, 273–275.

(4) Luan, B.; Robbins, M. *Nature* **2005**, *435*, 929–932.

(5) Mo, Y.; Turner, K.; Szlufarska, I. *Nature* **2009**, *457*, 1116–1119.

(6) Palacio, M. L. B.; Bhushan, B. *Crit. Rev. Solid State Mater. Sci.* **2010**, *35*, 73–104.

(7) Krautbauer, R.; Rief, M.; Gaub, H. E. *Nano Lett.* **2003**, *3*, 493–496.

(8) Vezenov, D. V.; Noy, A.; Rozsnyai, L. F.; Lieber, C. M. *J. Am. Chem. Soc.* **1997**, *119*, 2006–2015.

(9) Brewer, N.; Leggett, G. *Langmuir* **2004**, *20*, 4109–4115.

(10) Boyd, R. D.; Verran, J.; Jones, M. V.; Bhakoo, M. *Langmuir* **2002**, *18*, 2343–2346.

(11) Whitehead, K.; Rogers, D.; Colligon, J.; Wright, C.; Verran, J. *Colloids Surf., B* **2006**, *51*, 44–53.

(12) Williams, J. A.; Le, H. R. *J. Phys. D: Appl. Phys.* **2006**, *39*, R201–R214.

(13) Tambe, N. S.; Bhushan, B. *Ultramicroscopy* **2005**, *105*, 238–247.

(14) LaTorre, C.; Bhushan, B. *Ultramicroscopy* **2005**, *105*, 155–175.

(15) McMullen, R. L.; Kelty, S. P. *Scanning* **2001**, *23*, 337–345.

(16) Munz, M. *J. Phys. D: Appl. Phys.* **2010**, *43*, 1–34.

(17) Pettersson, T.; Nordgren, N.; Rutland, M. *Rev. Sci. Instrum.* **2007**, *78*, 093702.

(18) Wright, C. J.; Armstrong, I. *Surf. Interface Anal.* **2006**, *38*, 1419–1428.

(19) Cannara, R. J.; Eglin, M.; Carpick, R. W. *Rev. Sci. Instrum.* **2006**, *77*, 053701.

(20) Li, Q.; Kim, K. S.; Rydberg, A. *Rev. Sci. Instrum.* **2006**, *77*, 065105.

(21) Varenberg, M.; Etsion, I.; Halperin, G. *Rev. Sci. Instrum.* **2003**, *74*, 3362–3367.

(22) Asay, D. B.; Kim, S. H. *Rev. Sci. Instrum.* **2006**, *77*, 043903.

(23) Jeon, S.; Braiman, Y.; Thundat, T. *Appl. Phys. Lett.* **2004**, *84*, 1795–1797.

(24) Feiler, A.; Attard, P.; Larson, I. *Rev. Sci. Instrum.* **2000**, *71*, 2746–2750.

(25) Reitsma, M. G. *Rev. Sci. Instrum.* **2007**, *78*, 106102.

(26) Ecke, S.; Raiteri, R.; Bonaccurso, E.; Reiner, C.; Deiseroth, H. J.; Butt, H. J. *Rev. Sci. Instrum.* **2001**, *72*, 4164–4170.

(27) Green, C. P.; Lioe, H.; Cleveland, J. P.; Proksch, R.; Mulvaney, P.; Sader, J. E. *Rev. Sci. Instrum.* **2004**, *75*, 1988–1996.

(28) Ogletree, D. F.; Carpick, R. W.; Salmeron, M. *Rev. Sci. Instrum.* **1996**, *67*, 3298–3306.

(29) Stiernstedt, J.; Rutland, M. W.; Attard, P. *Rev. Sci. Instrum.* **2005**, *76*, 083710.

(30) Ruan, J. A.; Bhushan, B. *HTD (Am. Soc. Mech. Eng.)* **1994**, *116*, 378–388.

(31) Bennewitz, R. *Mater. Today* **2005**, *8*, 42–48.

(32) Matei, G.; Thoreson, E.; Pratt, J.; Newell, D.; Burnham, N. A. *Rev. Sci. Instrum.* **2006**, *77*, 1–6.

(33) Liu, J.; Grierson, D.; Moldovan, N.; Notbohm, J.; Li, S.; Jaroenapibal, P.; O'Connor, S.; Sumant, A.; Neelakantan, N.; Carlisle, J.; Turner, K.; Carpick, R. *Small* **2010**, *6*, 1140–1149.